ORIGINAL RESEARCH

CrossMark

Electronic structure and UV–Vis spectra simulation of square planar Bis(1-(4-methylphenylazo)-2-naphtol)-Transition metal complexes [M(L)$_2$]^x (M = Ni, Pd, Pt, Cu, Ag, and x = − 1, 0, + 1): DFT and TD-DFT study

Bachir Zouchoune [1,2] · Lakhdar Mansouri [1]

Abstract

DFT/B3LYP calculations with full geometry optimizations have been carried out on 1-phenylazo-2-naphthol and their metal complexes of formula M(MePhNap)$_2$ (M = Ni, Pd, Pt, Cu, Ag, and MePhNap = 1-(− 4-methylphenylazo)-2-naphtol) in their neutral, oxidized, and reduced forms. The predicted structures provide to the M(II) metal ions the square planar geometry and distorted azo ligand. The TD-DFT theoretical study performed on the optimized geometry allowed us to predict the UV–Vis spectra and to identify quite clearly the spectral position and the nature of the different electronic transitions according to their molecular orbital localization. Large HOMO-LUMO gaps are calculated for all optimized structures suggesting good chemical stabilities, hence, reproducing the available UV–Vis spectra and compared to that of free ligand. The electronic spectra obtained in DMSO and ethanol polar solvents predict more important red shifts than those obtained in hexane as nonpolar one.

Keywords Azo dye · Metal-ligand coordination · Electronic transitions · Molecular orbital localization

Introduction

Azo compounds are very important molecules and have been the subject of several works in both experimental and fundamental research [1, 2], where synthetic textile dyes of the azo family represent an important part of the world production of synthetic dyes and are characterized by the presence of the azo group (–N=N–) [3–5].

Azo derivatives and their metal complexes are essential pigments for synthetic leather and vinyl polymers. Furthermore, high-density optical data storage has been a focus of wide research in the past decades as nonlinear and photoelectronics [6]. Lately, metal complex dyes have also attracted increasing attention due to their interesting electronic and geometrical features in connection with their application for molecular memory storages, nonlinear optical elements, printing system, and so on [7–9].

Particularly, metal-azo complex dyes are used in the recording layer of DVD-R (Digital Versatile Disc-Recordable) disc, are lighter stable, allow for easier control of the wavelength by selection of the appropriate substituent groups, and have good thermal stability [10–16]. As known, the metal complex formation on chromophoric ligands leads to remarkable shift of UV–Vis absorption spectrum [9, 17–22] accompanied by the increasing of the dye fastness [21, 23].

The focus of this investigation is to give a deeper understanding on the coordination behavior of these azo molecules towards the M(II) (M = Ni, Pd, Pt, Cu, and Ag) metal ions using DFT and TD-DFT methods which are compared to the available experimental data and different analytical tools. Indeed, several experimental works have been the subject of syntheses, spectral characterizations, and X-ray diffraction of metal-azo complex dyes [24–34].

In addition, potentiometric and spectrophotometric investigations of Co^{2+}, Ni^{2+}, and Cu^{2+} metal cations connected to azo dyes have been reported [35]. Up till now, azo conjugated

✉ Bachir Zouchoune
  bzouchoune@gmail.com

1   Laboratoire de Chimie appliquée et Technologie des Matériaux, Université Larbi Ben M'Hidi - Oum El Bouaghi, (04000) Oum El Bouaghi, Algeria

2   Unité de Recherche de Chimie de l'Environnement et Moléculaire Structurale, Université Constantine (Mentouri), (25000) Constantine, Algeria

transition metal complexes have been shown to afford new possibilities en route for redox, optical properties, and magnetic due to the role of the *d* orbitals [9, 36–38].

In recent work, we have studied theoretically the substituent effects on 1-phenylazo-2-naphtol azo molecule substituted at the ortho position of the phenyl ring denoted (PhNap) as shown in Scheme 1 [39], while in this one, we will endeavor to provide an understanding into the *N,O*-bidentate chelation stabilization of 1-(4-methylphenylazo)-2-naphtol (MePhNap) as ligand in the M(MePhNap)$_2$ transition metal complexes. Furthermore, the relationship between the differences in absorption maximum from free ligand to their metal-azo complexes was thoroughly studied. It is worth noting that the organic ligands containing N and O donors give rise to great potential for fine control over coordination structural arrangements [40–46].

The density functional theory (DFT) method using the hybrid B3LYP functional or other hybrid and GGA ones is precious in determining the electronic structures, the geometrical parameters, the bonding, and other properties based on various works of monometallic systems [47–56].

Computational details

DFT calculations have been carried out on all complexes with the 2014.01 version of the Amsterdam Density Functional (ADF) program [57] developed by Baerends and co-workers [58–62]. All calculations have been performed with the hybrid-type B3LYP functional (Becke's three parameter hybrid exchange functional [63] coupled with the Lee-Yang-Parr nonlocal correlation functional) [64]. The atom electronic configurations were described by a triple-ζ Slater-type orbital (STO) basis set for H 1*s*, C 2*s* and 2*p*, and N 2*s* and 2*p* augmented with a 3*d* single-ζ polarization for C and N atoms and with a 2*p* single-ζ polarization for H atoms. A triple-ζ STO basis set was used for the first row transition metals Ni and Cu 3*d* and 4*s*, for second row Pd and Ag 4*d* and 5*s* and for third row Pt 5*d* and 6*s* augmented with a single-ζ, 4*p* polarization function for the first row Ni and Cu, a single-ζ, 5*p* polarization function for Pd and Ag and a single-ζ, 6*p* polarization function for Pt. For the systems containing atoms in which *Z* is greater than 41, the scalar relativistic zero-order
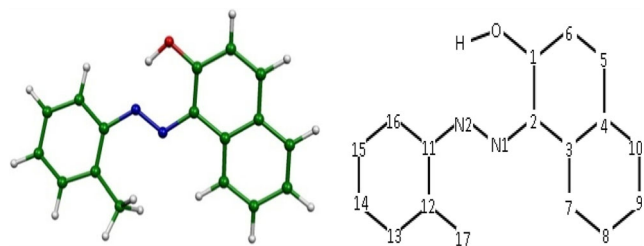
regular approximation (ZORA) was used (with the associated optimized valence basis set). Vibrational frequency calculation [65, 66] was performed on all the optimized geometries to verify that these structures are characterized as true minima on the potential energy surface. Singlet-triplet excitation energies and the transition dipole lengths were computed using TD-DFT as implemented in the response [67] code in the ADF package of programs.

The solvent effect using the Conductor-like Screening Model for Realistic Solvent (COSMO-RS) developed by Klamt and co-workers [68] was introduced in the single point DFT calculations, where the Cartesian coordinates were extracted from the geometry optimizations.
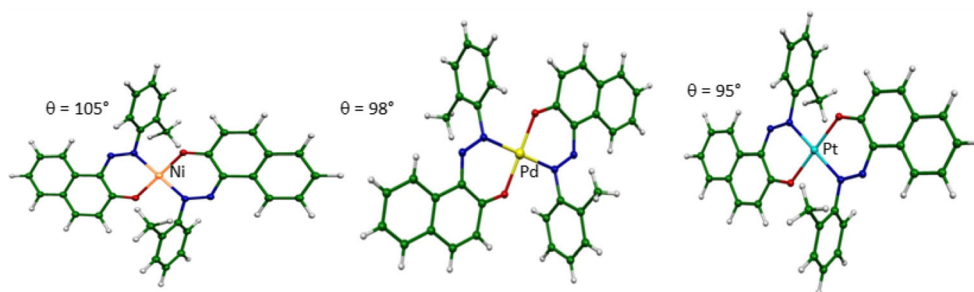
Representations of the molecular structures were done using the ADF-GUI [57] and the MOLEKEL4.1 [69] programs, respectively.

Results and discussion

Optimized structures and MO diagrams

The studied M(MePhNap)$_2$ compounds consist of slightly distorted square planar geometry of C_i symmetry, allowing considerable orbital mixing and more flexibility to the metal coordination sphere, where some of them are characterized experimentally [31, 32]. The full optimized geometry have been carried out on the diamagnetic Ni, Pd, and Pt metal species, where the two substituted azo ligands are symmetrical through an inversion center occupied by the metal cation which is tetraconnected via one N atom and one O atom of each azo dye molecule. Hence, our analysis has been extended to the paramagnetic Cu and Ag species. For all the studied complexes, the metal cation is connected to two molecules of (1-phenylazo-2-naphtol) through N and O atoms providing a square planar environment of the metal conducting to ML$_4$ complexes. The optimized geometries for Ni, Pd, and Pt complexes showed a perfect square planar arrangement around the M(II) metal cation as sketched in Fig. 1, while the azo ligand undergoes substantial modifications losing its nearly flatness as displayed in Scheme 1 and Fig. 1, because of the fixation of coordinative bonds and the geometric requirement for the central M(II) square plane. The planarity of the different ML$_4$ complexes around the metal is highlighted by the ONON dihedral angle of 0° and the linear O–M–O and N–M–N bond angles of 180° for Ni, Pd, and Pt complexes, in accordance with the 16-MVE (metal valence electrons) configuration of the Ni(II), Pd(II), and Pt(II) as d^8 metal cations. The computed M–N bond distances of 1.919, 2.101, and 2.108 Å and M–O bond distances of 1.842, 2069, and 2.077 Å for Ni, Pd, and Pt complexes, respectively, are in harmony with the increasing of the metal radii following the order: Ni < Pd < Pt. It is worth nothing that for the Pd structure, the optimized parameters are

Scheme 1 the Optimized structure of (1-(4-methylphenylazo)-2-naphtol) denoted (MePhNap) and its atoms numbering

comparable to those observed experimentally [31] as gathered in Table 1 and comparable to those reported in recent work [33, 34]. The calculated C–C bond distances ranging from 1.38 to 1.42 Å (Scheme 1) suggest a delocalized scheme within the phenyl and naphtyl rings for Ni, Pd, and Pt complexes as shown in Fig. 1. As clearly shown in Fig. 1, both azo dye molecules are oriented to each other by 105, 98, and 95° for Ni, Pd, and Pt species, respectively, due to the steric repulsions, thus avoiding the planarity of the different complexes. It is important to note that the orientation between the azo ligands is more marked for the 3*d* Ni transition metal than those of 4*d* and 5*d* ones. The N–N bond distance of 1.269 Å for the azo group in the free molecule undergo lengthening for Ni complex becoming equal to 2.272 Å, but slightly shortened in Pd and Pt complexes becoming equal to 2.266 and 2.265 Å, respectively. The MO diagrams for the diamagnetic Ni(MePhNap)₂, Pd(MePhNap)₂, and Pt(MePhNap)₂ complexes are shown in Fig. 2, exhibiting large HOMO-LUMO gaps of 3.15, 3.08, and 3.07 eV, respectively, suggesting good chemical stability. For the three neutral Ni(MePhNap)₂, Pd(MePhNap)₂, and Pt(MePhNap)₂ complexes, the LUMOs are ligand character, while the HOMOs are weakly metallic orbitals showing a contribution not exceeding 10% in each case. It is interesting to note that the orbitals with considerable metal based are located relatively at low energies, particularly, $71a_g$ (31%), $73a_g$ (15%), and $74a_g$ (40%) for Ni(MePhNap)₂; $71a_g$ (30%), $73a_g$ (35%), and $74a_g$ (30%) for Pd(MePhNap)₂; and $71a_g$ (30%), $71a_g$ (30%), $73a_g$ (20%), and $74a_g$ (20%) for Pt(MePhNap)₂ which are principally nonbonding orbitals.

The optimized geometry of the paramagnetic Cu(MePhNap)₂ and Ag(MePhNap)₂ complexes are sketched in Fig. 3 and Fig. 4. For the optimized neutral Cu(MePhNap)₂ structure having 17-MVE configuration in its doublet spin state (*S* = ½), the Cu–N and Cu–O bond distances of 2.020 and 1.921 Å are comparable to the experimental ones of average values of 1.999 and 1.924 Å, respectively, and the N–Cu–N and O–Cu–O bond angles are of 180° [32]. The NONO plane centered by the copper dication of 0° corresponds to ML₄ square planar geometry, while the azo dye molecules are oriented to each other by 98°. The one electron oxidation gives rise to the [Cu(MePhNap)₂]⁺ structure of 16-MVE configuration which is isoelectronic with the neutral Pd and Pt complexes and exhibiting a significant HOMO-LUMO gap of

1.66 eV as clearly shown in Fig. 5. This oxidation leads to the Cu–N and Cu–O bond distances lengthening from 2.020 and 1.921 Å to 2.259 and 1.983 Å, respectively, but keeping the same square planar geometry. The neutral Ag(MePhNap)₂ 17-MVE structure consists of an ML₄ square plane, in which the N–Ag–N and O–Ag–O are linear and Ag–N and Ag–O bond distances are of 2.275 and 2.215 Å. The one electron reduction of the square plane Ag(MePhNap)₂ structure without any symmetry constraints gives rise to the anionic [Ag(MePhNap)₂]⁻ structure undergoing a considerable distortion as shown in Fig. 4, wherein the N–Ag–N and O–Ag–O of 159 and 124° deviate considerably from the linearity, in accordance with the 18-MVE configuration of a tetrahedral ML₄ complex around the Ag⁺ center, in which the N–Ag and O–Ag bond distances undergo considerable lengthening from 2.275 and 2.215 to 2.440 and 2.376 Å, respectively, in agreement with the population of the antibonding $83a_g$ orbital as shown by the MOs diagram of Fig. 5. However, the [Ag(MePhNap)₂]⁺ structure keeps the same square plane geometry, but accompanied by slight shortening of N–Ag and O–Ag bond distances. It is noticeable that the redox property studies of Cu complexes are showing the irreversible character [70].

Electronic spectra

In order to gain a better understanding of the simulated UV–Vis spectra, TD-DFT calculations were carried out on the MePhNap azo dye molecule substituted at the ortho position of the phenyl by CH₃ and their transition metal M(MePhNap)₂ (*M* = Ni, Pd, and Pt) complexes. The theoretical electronic spectrum (Fig. 6a) of the substituted azo dye in gas phase displays a major band in the region of 420–445 nm due to the $(\pi_{C-C} + n) \rightarrow (\pi^*_{N-N} + \pi^*_{C-O})$ and $\pi_{C-C} \rightarrow (\pi^*_{N-N} + \pi^*_{C-O})$ transitions corresponding to the HOMO-1→LUMO (81%) and HOMO-LUMO (15%) electronic transitions with an oscillator strength of 0.42 (a.u), implying the naphtyl ring and the –N=N– azo group as intramolecular charge transfer (ILCT). Whereas, the theoretical electronic spectra of the studied azo dye exhibit red shifts in different used solvents (Fig. 6a). Really, one can observe that the polar DMSO and ethanol solvents conduct to similar spectra, where the main pick is moved to the region of 480–512 nm with an oscillator

Table 1 Selected geometrical and energetic parameters for neutral M(MePhNap)$_2$ (M = Ni, Pd, Pt, Cu, Ag), cationic [M(MePhNap)$_2$]$^+$ (M = Cu, Ag), and anionic [Ag(MePhNap)$_2$]$^-$ complexes of different metal valence electrons (MVE). The HOMO-LUMO gap is given in (eV), and total bonding energy is given in (kcal/mol)

Complex	Ag(MePhNap)$_2$	[Ag(MePhNap)$_2$]$^+$	[Ag(MePhNap)$_2$]$^-$	Cu(MePhNap)$_2$	[Cu(MePhNap)$_2$]$^+$	Ni(MePhNap)$_2$	Pt(MePhNap)$_2$	Pd(MePhNap)$_2$
MVE	17	16	18	17	16	16	16	16
Spin state	S = 1/2	S = 0	S = 0	S = 1/2	S = 0	S = 0	S = 0	S = 0
HOMO-LUMO gap	1.64	1.12	3.12	3.32	1.69	3.15	3.08	3.07
Total bonding energy	−11,578.3	−11,437.2	−11,655.1	−11,627.5	−11,475.6	−11,722.5	−11,608.8	−11,688.1
Bond length (Å)								
C(2)–N(1)	1.346	1.335	1.357	1.346 (1.366)	1.329	1.347	1.35 (1.371)	1.351
N(1)–N(2)	1.263	1.259	1.279	1.271 (1.274)	1.259	1.272	1.265	1.266 (1.279)
C(11)–N(2)	1.432	1.413	1.422	1.446 (1.452)	1.442	1.453	1.444	1.444 (1.451)
C(11)–C(12)	1.404	1.412	1.408	1.398 (1.386)	1.400	1.397	1.397	1.399 (1.391)
M–O	2.215	2.159	1.422	1.921 (1.924)	1.847	1.842	2.077	2.069 (1.969)
C(1)–O	1.271	1.274	1.262	1.236 (1.309)	1.290	1.286	1.284	1.284 (1.284)
Bond angle (°)								
C(2)–N(1)–N(2)	125 .2	213.5	123.2	127.5	124.3	123.6	125.9	126.0
N(1)–N(2)–M	134.5	122.7	126 .6	125 .1	127.9	128.2	127.2	127.1
N(2)–M–O	74	79	72	91	89	92	89	88
Dihedral angle (°)								
N(2)–O–N(2)–O'	0	0	54	0	0	0	0	0

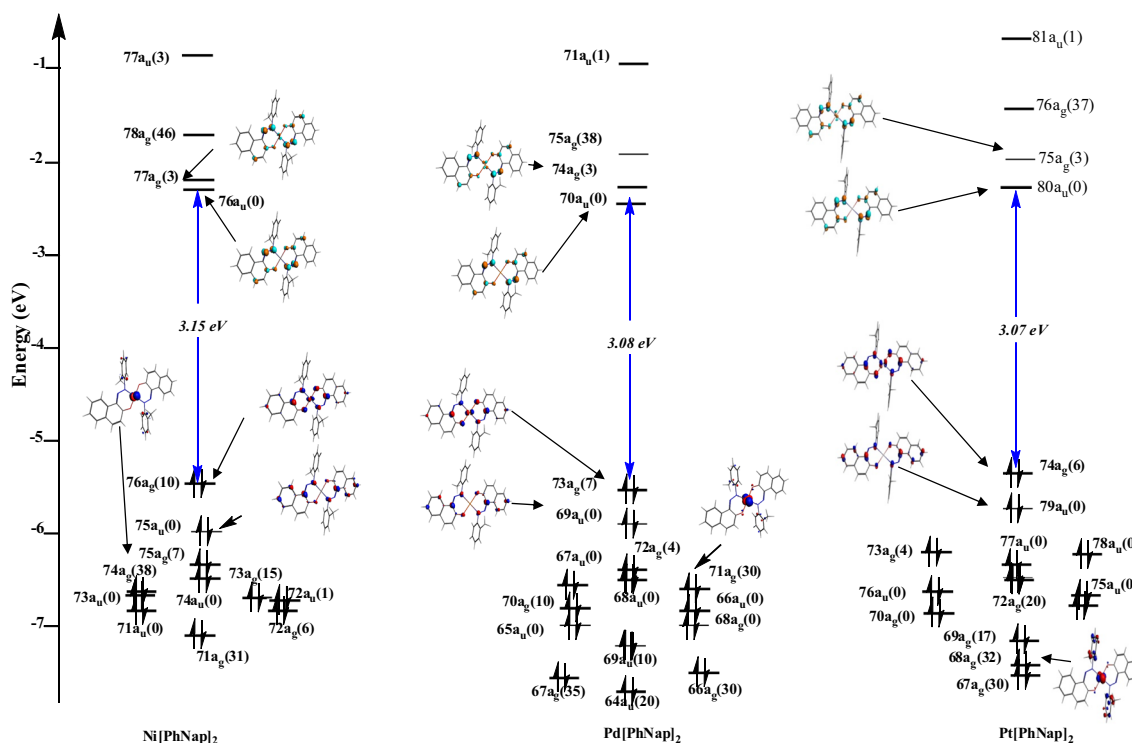**Fig. 2** MO diagrams of M(MePhNap)2 (M = Ni, Pd, Pt). The metal contributions in (%) are given in parentheses

strength of 0.8 (a.u). Since they have sharp UV–Vis spectra that are tremendously sensitive to the immediate environment, like as the solvent polarity phenomenon, which is known for many dye molecules [71, 72]. The electronic spectrum obtained in hexane solvent is slightly shifted to the region of 445–470 nm with oscillator strength of 0.6 (a.u), which is comparable to the experimental results found by V.N. Mkpenie et al., where the main peak is shifted from 450 to 460 nm [73]. It is worth noting that the same orbitals are implied in the electronic transitions both in gas phase and in the different solvents used, but exhibiting differences in their contribution as clearly shown in Table 2.

The three electronic spectra of Ni, Pd, and Pt diazo complexes exhibit similar shapes, but with somewhat differences concerning the bands' positions and their widths (Fig. 6b, c, d). Our spectral analysis is based on the comparison of the

theoretical spectra obtained for the uncomplexed and the complexed species in gas phase and in different solvents as shown in Fig. 6, while the identification of the electronic transitions are based on the MOs' localization. Indeed, different from the electronic spectrum of the (MePhNap) azo dye molecule, one can observe the appearance of new bands and the weakness of others. Because M(MePhNap)$_2$ complexes are constructed from two bidentate π-conjugated (MePhNap) azo ligands connected to one transition metal, different electronic transitions should appear; these can be probably classified into metal to ligand charge transfer (MLCT), ligand to metal CT (LMCT), intrametal d–d* orbitals, intraligand, and interligand transitions. The calculated transitions have been assigned to these classes (Tables 3, 4, 5) by TD-DFT analysis based on the orbital characteristics (Fig. 6). For the Ni complex spectrum (Fig. 6b), the main absorption band appears essentially in the

Fig. 3 Optimized [Cu(MePhNaph)$_2$]$^+$ and Cu(MePhNaph)$_2$ structures of doublet (S = 1/2) (**a**) and singlet (S = 0) (**b**) spin states, respectively
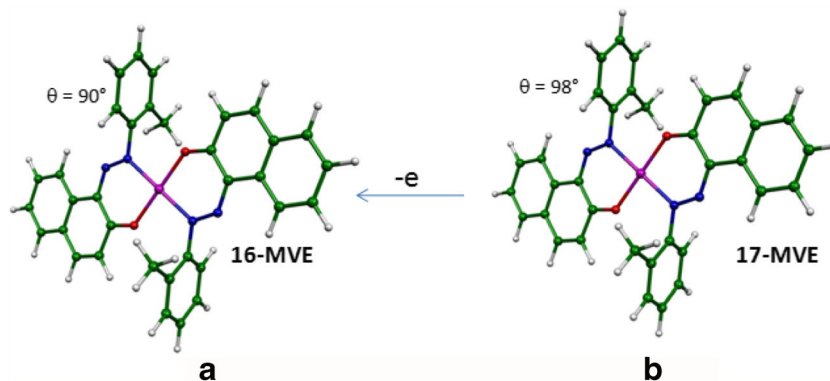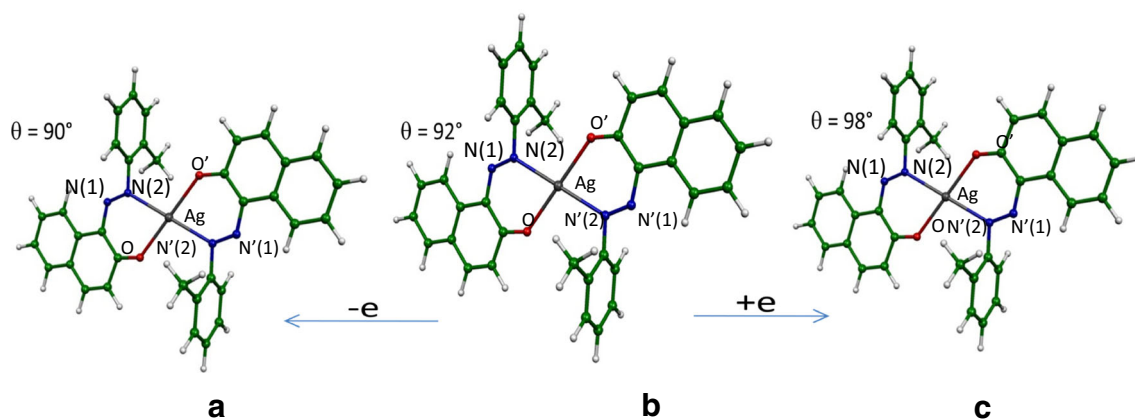
Fig. 4 Optimized [Ag(MePhNaph)$_2$]$^+$ (**a**), Ag(MePhNaph)$_2$ (**b**), and [Ag(MePhNaph)$_2$]$^-$ (**c**) structures of 16-, 17-, and 18-MVEs, respectively

ultraviolet region centered at 370, 374, 382, and 382 nm in gas phase, hexane, ethanol, and DMSO, respectively, corresponding to the intense $(d(M) + \pi) \rightarrow \pi^*$ transitions, which are remarkably reinforced (Table 3). These transitions are metal-ligand and intraligand characteristics corresponding to excitations from the metal and the MePhNap's HOMO (76a$_g$ which is made of a mixture of d metallic, nitrogen and oxygen orbitals) to LUMO (76a$_u$ which is purely ligand). While the relatively weak band appearing in the visible region and centered at 476, 477, 482, and 482 nm in gas phase, hexane, ethanol, and DMSO, respectively, is established between the

HOMO (76a$_g$) and the LUMO (76a$_u$) electronic transition with and can be classified into metal to ligand charge transfer (MLCT) and intraligand charge transfer (ILCT). It is noteworthy that the electronic transitions are intensified in polar solvents rather than in both nonpolar one and in gas phase.

For the Pd complex spectrum (Fig. 6c), the main absorption band appears essentially in the ultraviolet region centered at 370, 373, 379, and 379 nm in gas phase, hexane, ethanol, and DMSO, respectively, corresponding to the intense $(d(M) + \pi(L)) \rightarrow \pi^*(L)$ transitions, which are considerably enhanced in intensity (Table 4) compared to those
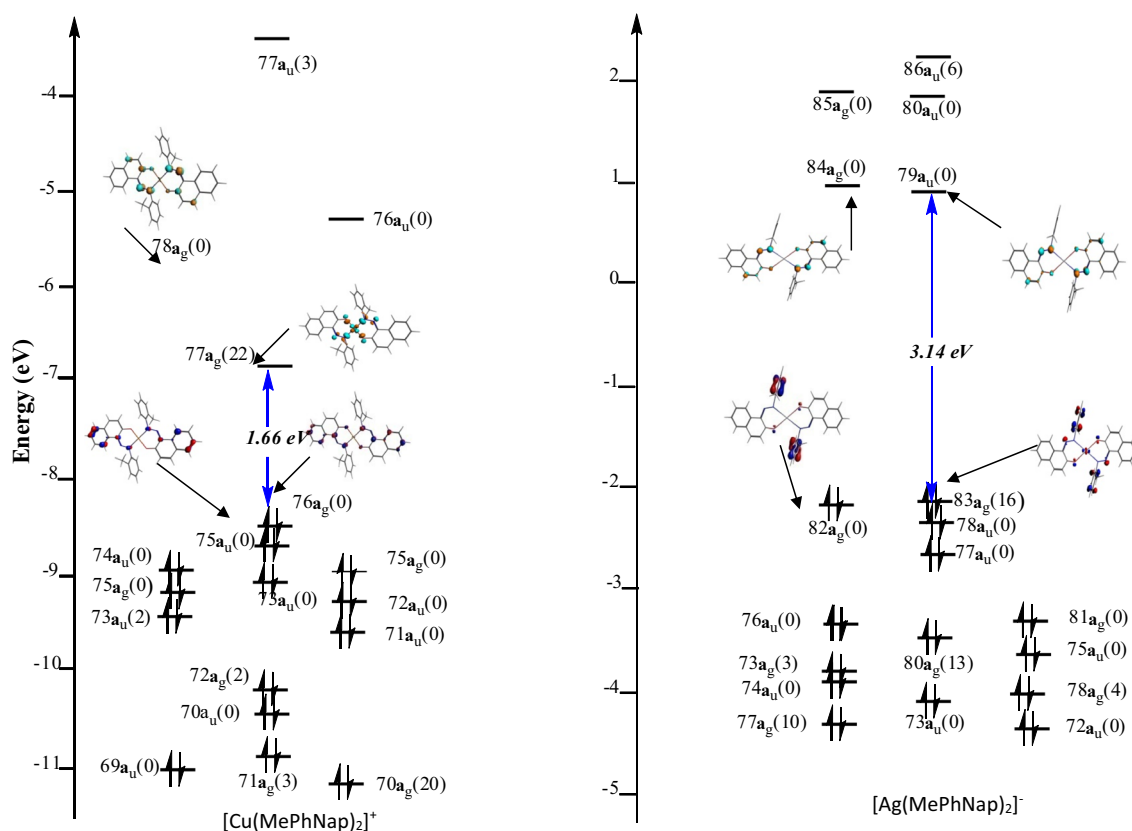

Fig. 5 MO diagrams of [Cu(MePhNap)2]$^+$ and [Ag(MePhNap)2]$^-$. The metal contributions in (%) are given in parentheses
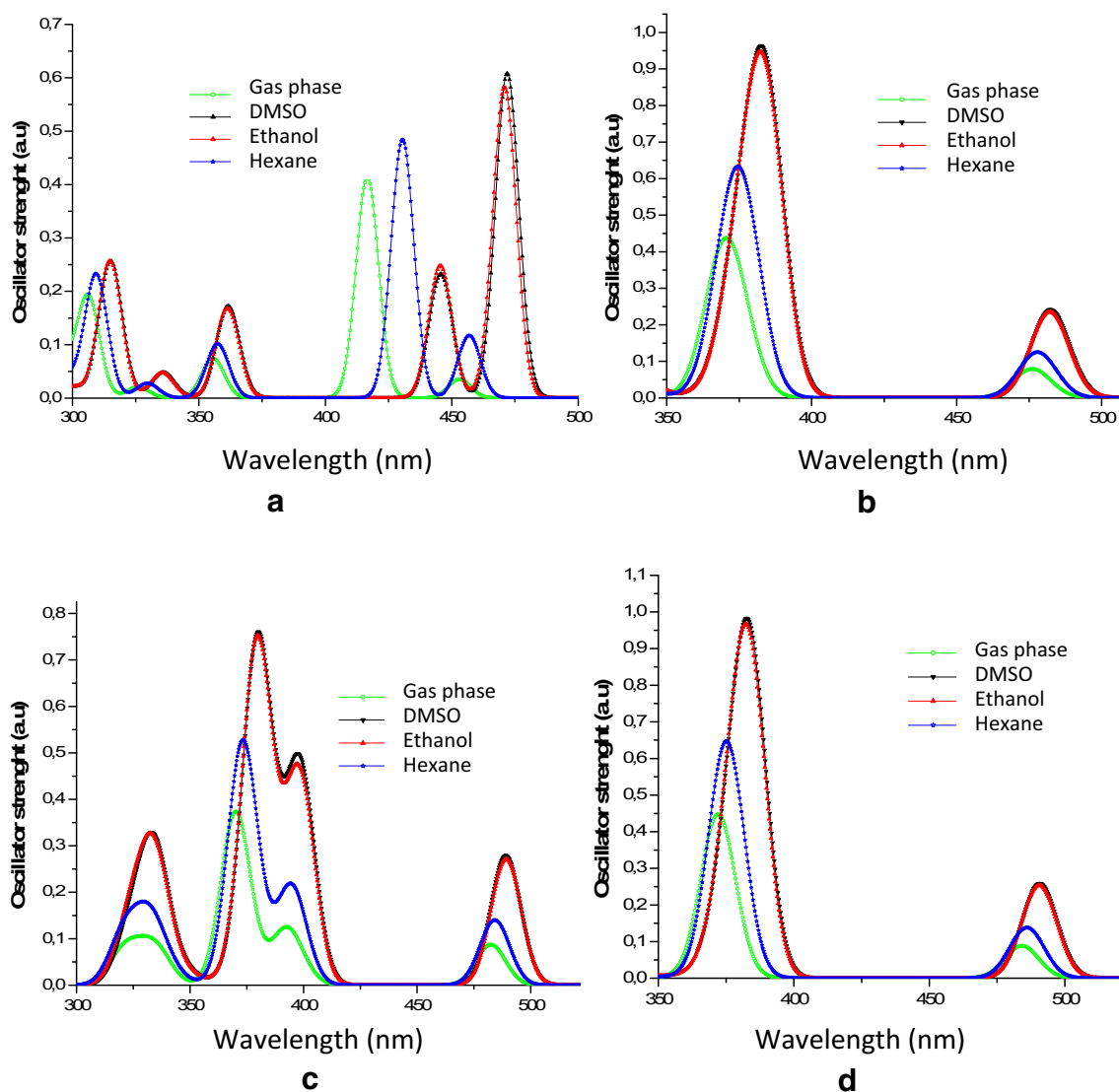
Fig. 6 Electronic spectra of **a**, **b**, **c**, and **d** obtained in gas phase and different solvents for the uncomplexed azo dye, Ni, Pd, and Pt complexes, respectively

Table 2 Calculated electronic transitions and their assignments, the dominant contributions to electron excitations in percentages (%), wavelengths λ (nm), oscillator strengths f (au), and excitation energies ΔE (eV) for uncomplexed (MePhNap) species obtained in gas phase and different solvents

Band	Solvent	λ	ΔE	f	Electronic transition (%)	Assignment
A	Gas phase	453	4.0	0.0351	68a→70a (81)	$\pi + n \rightarrow \pi^*$
			3.2		69a→70a (15)	
	DMSO	472	3.3	0.6085	69a→70a (76)	$\pi + n \rightarrow \pi^*$
			3.8		68a→70a (22)	
	Ethanol	470	3.2	0.5826	69a→70a (74)	$\pi + n \rightarrow \pi^*$
			4.0		68a→70a (25)	
	Hexane	457	4.0	0.1171	68a→70a (69)	$\pi + n \rightarrow \pi^*$
			3.2		69a→70a (22)	
B	Gas phase	416	3.2	0.4130	69a→70a (88)	$\pi + n \rightarrow \pi^*$
			3.9		68a→70a (10)	
	DMSO	445	3.8	0.2324	68a→70a (70)	$\pi + n \rightarrow \pi^*$
			3.2		69a→70a (23)	
	Ethanol	445	4.0	0.2408	68a→70a (69)	$\pi + n \rightarrow \pi^*$
			3.3		69a→70a (25)	
	Hexane	430	3.2	0.4844	69a→70a (76)	$\pi + n \rightarrow \pi^*$
			4.0		68a→70a (22)	

Table 3 Calculated electronic transitions and their assignments, the dominant contributions to electron excitations in percentages (%), wavelengths λ (nm), oscillator strengths f (au), and excitation energies ΔE (eV) of Ni(MePhNap)$_2$ complexes obtained in gas phase and different solvents. The oscillator strength values less than 0.05 (au) are not listed

Band	Solvent	λ	ΔE	f	Electronic transition (%)	Assignment
A	Gas phase	476	3.20	0.079	$76a_g \rightarrow 76a_u$ (95)	$d(M) + \pi(L) \rightarrow \pi^*(L)$
	DMSO	482	3.17	0.2452	$76a_g \rightarrow 76a_u$ (97)	$d(M) + \pi(L) \rightarrow \pi^*(L)$
	Ethanol	482	3.14	0.2352	$76a_g \rightarrow 76a_u$ (95)	$d(M) + \pi(L) \rightarrow \pi^*(L)$
	Hexane	477	3.17	0.1253	$76a_g \rightarrow 76a_u$ (93)	$d(M) + \pi(L) \rightarrow \pi^*(L)$
B	Gas phase	370	3.74	0.4379	$75a_u \rightarrow 77a_g$ (90)	$d(M) + \pi(L) \rightarrow$
			4.26		$74a_u \rightarrow 76a_u$ (2)	$\pi^*(L) + d(M)$
			5.01		$72a_u \rightarrow 78a_g$ (17)	
			3.94		$75a_u \rightarrow 76a_u$ (87)	
	DMSO	382	4.61	0.9635	$75a_u \rightarrow 77ag$ (52)	$d(M) + \pi(L) \rightarrow$
			3.95		$75a_u \rightarrow 76a_u$ (40)	$\pi^*(L) + d(M)$
			4.26		$74a_u \rightarrow 77a_g$ (3)	
			4.05		$73a_g \rightarrow 76a_u$ (2)	
	Ethanol	382	3.77	0.9484	$75a_u \rightarrow 77a_g$ (43)	$d(M) + \pi(L) \rightarrow$
			3.95		$75a_g \rightarrow 76a_u$ (38)	$\pi^*(L) + d(M)$
			4.22		$74a_u \rightarrow 77a_g$ (3)	
	Hexane	374	3.75	0.6332	$75a_u \rightarrow 77a_g$ (74)	$d(M) + \pi(L) \rightarrow$
			3.95		$75a_g \rightarrow 76a_u$ (15)	$\pi^*(L) + d(M)$
			4.27		$73a_g \rightarrow 76a_u$ (5)	

obtained for the uncomplexed species. These transitions are metal-ligand and intraligand characteristics stemming from the metal and the MePhNap's HOMO-3 ($72a_g$ which is made of a mixture of d metallic, nitrogen, and oxygen orbitals) to LUMO ($70a_u$ which is purely ligand) featuring the principally transition (72%) and coupled to two others

Table 4 Calculated electronic transitions and their assignments, the dominant contributions to electron excitations in percentages (%), wavelengths λ (nm), oscillator strengths f (au), and excitation energies ΔE (eV) of Pd[MePhNap]$_2$ complexes obtained in gas phase and different solvents. The oscillator strength values less than 0.05 (au) are not listed

Band	Solvent	λ	ΔE	f	Electronic transition (%)	Assignment
A	Gas phase	482	3.08	0.0872	$73a_g \rightarrow 70a_u$ (96)	$d(M) + \pi(L) \rightarrow \pi^*(L)$
	DMSO	489	3.11	0.2794	$73a_g \rightarrow 70a_u$ (97)	$d(M) + \pi(L) \rightarrow \pi^*(L)$
	Ethanol	489	3.11	0.2722	$73a_g \rightarrow 70a_u$ (97)	$d(M) + \pi(L) \rightarrow \pi^*(L)$
	Hexane	484	3.09	0.1413	$73a_g \rightarrow 70a_u$ (97)	$d(M) + \pi(L) \, \pi^*(L)$
B	Gas phase	370	3.88	0.3725	$72a_g \rightarrow 70a_u$ (79)	$d(M) + \pi(L) \rightarrow \pi^*(L)$
			4.11		$71a_g \rightarrow 70a_u$ (11)	
			4.18		$68a_u \rightarrow 74a_g$ (6)	
			4.61		$73a_g \rightarrow 71a_u$ (2)	
	DMSO	379	3.89	0.7604	$72a_g \rightarrow 70a_u$ (72)	$d(M) + \pi(L) \rightarrow \pi^*(L)$
			4.27		$67a_u \rightarrow 74a_g$ (11)	
			4.08		$71a_g \rightarrow 70a_u$ (6)	
			4.20		$68a_u \rightarrow 74a_g$ (3)	
	Ethanol	379	3.89	0.7526	$72a_g \rightarrow 70a_u$ (73)	$d(M) + \pi(L) \rightarrow \pi^*(L)$
			4.27		$67a_u \rightarrow 74a_g$ (11)	
			4.08		$71a_g \rightarrow 70a_u$ (6)	
			4.20		$68a_u \rightarrow 74a_g$ (3)	
	Hexane	373	3.89	0.5277	$72a_g \rightarrow 70a_u$ (80)	$d(M) + \pi(L) \rightarrow \pi^*(L)$
			4.09		$71a_g \rightarrow 70a_u$ (7)	
			4.28		$67a_u \rightarrow 74a_g$ (6)	
			4.19		$68a_u \rightarrow 74a_g$ (8)	
			3.65		$66a_u \rightarrow 74a_g$ (6)	

Table 5 Calculated electronic transitions and their assignments, the dominant contributions to electron excitations in percentages (%), wavelengths λ (nm), oscillator strengths f (au), and excitation energies ΔE (eV) of Pt[MePhNap]$_2$ complexes obtained in gas phase and in different solvents. The oscillator strength values less than 0.05 (au) are not listed

Band	Solvent	λ	ΔE	f	Electronic transition (%)	Transition assignment
A	Gas phase	484	3.072	0.0889	$74a_g \rightarrow 80a_u(97)$	$d(M)+\pi(L)\rightarrow\pi^*(L)$
	DMSO	490	3.100	0.2604	$74a_g \rightarrow 80a_u$ (98)	$d(M)+\pi(L)\rightarrow\pi^*(L)$
	Ethanol	490	3.112	0.2539	$74a_g \rightarrow 80a_u$ (98)	$d(M)+\pi(L)\rightarrow\pi^*(L)$
	Hexane	484	3.084	0.1388	$74a_g \rightarrow 80a_u$ (97)	$d(M)+\pi(L)\rightarrow\pi^*(L)$
B	Phase gazeuse	372	3.86	0.4448	$73a_g \rightarrow 80a_u$ (72)	$\pi(L)\rightarrow\pi^*(L)$
			3.76		$79a_u \rightarrow 75a_g$ (8)	
			4.34		$77a_u \rightarrow 75a_g$ (6)	
			4.21		$72a_g \rightarrow 80a_u$ (4)	
	DMSO	382	3.88	0.9833	$73a_g \rightarrow 80a_u$ (67)	$\pi(L)\rightarrow\pi^*(L)$
			3.79		$79a_u \rightarrow 75a_g$ (21)	
			4.27		$78a_u \rightarrow 75a_g$ (7)	
	Ethanol	382	3.88	0.9675	$73a_g \rightarrow 80a_u$ (67)	$d(M)+\pi(L)\rightarrow\pi^*(L)$
			3.79		$79a_u \rightarrow 75a_g$ (22)	
			4.28		$78a_u \rightarrow 75a_g$ (7)	
			4.89		$72a_g \rightarrow 80a_u$ (8)	
	Hexane	375	3.87	0.6462	$73a_g \rightarrow 80a_u$ (56)	$d(M)+\pi(L)\rightarrow\pi^*(L)$
			4.32		$77a_u \rightarrow 75a_g$ (17)	
			4.18		$72a_g \rightarrow 80a_u$ (10)	
			4.21		$79au \rightarrow 75a_g$ (31)	
			4.29		$71a_g \rightarrow 80a_u$ (5)	

less intense as specified in Table 4. The band found at relatively low energy centered at 482, 484, 489, and 489 nm in gas phase, hexane, ethanol, and DMSO, respectively, occurred chiefly between the HOMO ($73a_g$) and the LUMO ($70a_u$) corresponding to the metal to ligand charge transfer (MLCT) and intraligand charge transfer (ILCT), where the λ_{max} is reached for the polar DMSO and ethanol solvents for oscillator strength values of 0.28 and 0.27 (a.u). Finally, in the electronic spectrum of azo-Pt complex (Fig. 6d), the absorption band A in the visible region at 476 nm in gas phase corresponds to the $(d(M)+n)\rightarrow$ $(\pi^*_{N-N}+\pi^*_{C-O})$ electronic transition assigned to HOMO→LUMO transition, which is shifted by about 51 nm than that of the free ligand as is aforementioned. In the gas phase, the strong absorption band appears in the ultraviolet region centered at 370 nm.

Also, it is worthwhile to mention the weak ligand to metal charge transfer LMCT occurred from the ligand orbitals to $78a_g$, $75a_g$, and $76a_g$ as LUMO+2 for Ni, Pd, and Pt complexes, respectively, which feature considerable metal contributions as shown in Fig. 3.

Conclusion

In this theoretical investigation, we have shown that the geometry of free ligand does not deviate from the planarity which exhibits a delocalized scheme within both phenyl and naphtyl rings connected to each other by the azo –N=N– group.

Once the azo ligand is complexed, it could not maintain the approximate planar structure and the dihedral angles between the phenyl and naphtyl rings become almost perpendicular evidenced by the dihedral angle value of about 95° in the M(MePhNap)$_2$ (M = Ni, Pd, Pt, Cu, and Ag) complexes, which are comparable to the available Pd and Cu experimental data. Whereas, the metal M(II) cation is in a perfect square planar environment as an ML$_4$ fragment obeying the 16-MVE configuration and the different computed structures display large HOMO-LUMO gaps. The reduced [Ag(MePhNap)$_2$]$^-$ species underwent a geometrical distortion from ML$_4$ with 17-MVE square planar to ML$_4$ tetrahedral structure obeying the 18-MVE rule. From the electronic spectra obtained for the Ni, Pd, and Pt complexes, one can observe that the main peaks are attributed to the HOMO→LUMO and HOMO-1→ LUMO electronic transitions. Based on the obtained HOMO-LUMO gaps and the electronic spectra for the metal-azo complexes, slight bathochromic shifts are observed towards the long wavelengths with diminution of the HOMO-LUMO energy gaps; thus, the enhancement of the wavelengths pursues the following sequence: Ni < Pd < Pt.

References

1. Zollinger H (1987) Color chemistry. VCH Publishers, New York

2. Nishihara H (2004) Multi-mode molecular switching properties and functions of azo-conjugated metal complexes. Bull Chem Soc Jpn 77:407

3. Tincher WC (1989) Processing wastewater from Carpet Mills. Text Chem Color 21:33

4. Morrison C, Bandara J, Kiwi J (1996) Sunlight induced decoloration/degradation of non-biodegradable orange II dye by advanced oxidation technologies in homogeneous and heterogeneous media. J Adv Oxid Technol 1:160

5. Nadtochenko V, Kiwi J (1997) Photoinduced adduct formation between orange II and [Fe 3+(aq)] or Fe(ox) 3 3−H₂O₂ photocatalytic degradation and laser spectroscopy. J Chem Soc Faraday Trans 93:2373

6. Katz HE, Singer KD, Sohn JE, Dirk CW, King LA, Gordon HM (1987) Greatly enhanced second-order nonlinear optical susceptibilities in donor-acceptor organic molecules. J Am Chem Soc 109:6561

7. Abe T, Mano S, Yamada Y, Tomotake A (1999) Termal dye transfer printing with chelate compounds. J Imag Sci Technol 43:339

8. Wang S, Shen S, Xu H (2000) Synthesis spectroscopic and thermal properties of a series of azo metal chelate dyes. Dyes Pigments 44:195

9. Wu S, Qian W, Xia Z, Zou Y, Wang S, Shen S (2000) Investigation of third-order nonlinearity of an azo dye and its metal-substituted compounds. Chem Phys Lett 330:535

10. Geng Y, Gu D, Gan F (2004) Application of novel azo metal thin film in optical recording. Opt Mater 27:193

11. Bin W, Yi-Qun W, Dong-Hong G, Fu-Xi G (2003) Optical parameters and absorption of azo dye and its metal-substituted compound thin films. Chin Phys Lett 20:1596

12. Fu-Xin H, Yi-Qun W, Dong-Hong G, Fu-X G (2003) Spectroscopy and optical properties of novel metal(II)-azo complex films in blue-violet light region. Chin Phys Let 20: 2259

13. Hamada E, Fujii T, Tomizawa Y, Iimura S (1997) High density optical recording on dye material discs: an approach for achieving 4.7 GB density. Jpn J Appl Phys 36:593

14. Suzuki Y, Okamoto Y, Kurose Y, Maeda S (1999) High-speed recording performance of metal azo dye containing digital video disc-recordable discs. Jpn J Appl Phys 38:1669

15. Nejati K, Rezvani Z, Seyedahmadian M The synthesis, characterization, thermal and optical properties of copper, nickel, and vanadyl complexes derived from azo dyes. Dyes Pigments 83:304

16. Li X, Wu Y, Gu D, Gan F (2010) Spectral, thermal and optical properties of metal(II)–azo complexes for optical recording media. Dyes Pigments 86:182

17. Woodward C, Freiser H (1973) Sulphonated azo-dyes as extractive metallochromic reagents. Talanta 20:417

18. Shibata S, Furukawa M, Toei K (1973) Syntheses and spectrophotometric studies of azo dyes containing *m*-dimethylaminophenol as analytical reagents. Anal Chim Acta 66:397

19. Pilipenko AT, Savransky LI (1987) Selectivity and sensitivity of metal determination by co-ordination compounds. Talanta 34:77

20. Szurdoki F, Ren D, Walt DR (2000) A combinatorial approach to discover new chelators for optical metal ion sensing. Anal Chem 72:5250

21. Abe T, Mano S, Yamaya Y, Tomotake A (1999) Thermal dye transfer printing with chelate compounds. J Imag Sci Tech 43:339

22. Meyers GA, Michaels FM, Reeves RL, Trotter P (1985) Kinetics and mechanism of chelation of nickel(II) by a tridentate .alpha.-[(2-hydroxyphenyl)azo]-.alpha.-acetoacetonitrile and an .alpha.-(8-quinolylazo)-.alpha.-acetoacetonitrile dye. J Inorg Chem 24:731

23. Graves HM, Johnston LG, Reiser A (1988) The effect of metallization on singlet oxygen formation by azo-dyes. J Photochem Photobiol A 43:183

24. M. A Benaouida, A. Benosmane, H. Bouguerria, S. E Bouaoud, H. Merazig. Bis{1-[(*E*)-(2-chlorophenyl)diazenyl]naphthalen-2-olato}copper(II). Acta Cryst E69 (2013) m405

25. Kurahashi M (1974) Crystal structure of bis(1-(2-thiazolylazo)-2-naphtolato)nickel(II). Bul Chem Soc Jpn 47:2067

26. Jarad AJ, Majeed IY, Hussein AO (2018) Synthesis and spectral studies of heterocyclic azo dye complexes with some transition metals. J Phys Conf Ser 1003:012021

27. Kilinçarslan R, Erdem E (2007) Synthesis and spectral characterization of some new azo dyes and their metal complexes. Transit Met Chem 32:102

28. Abdallah SM (2012) Metal complexes of azo compounds derived from 4-acetamidophenol and substituted aniline. Arab J Chem 5:251

29. Gup R, Giziroglu E, Kırkan B (2007) Synthesis and spectroscopic properties of new azo-dyes and azo-metal complexes derived from barbituric acid and aminoquinoline. Dyes Pigments 73:40

30. Chen XC, Tao T, Wang YG, Peng YX, Huang W, Qian HF (2012) Azo-hydrazone tautomerism observed from UV-Vis spectra by pH control and metal-ion complexation for two heterocyclic disperse yellow dyes. Dalton Trans 41:11107

31. Lin ML, Tsai CY, Li CY, Huang BH, Ko BT (2010) Bis{1-[(E)-(2-methyl-phen-yl)diazen-yl]-2-naphtho-lato}palladium(II). Acta Cryst E 66:m1022

32. Tai WJ, Li CH, Li CY, Ko BT (2010) Bis{1-[(E)-o-tolyl-diazen-yl]-2-naphtho-l-ato}copper(II). Acta Cryst E 66:m1315

33. Chetioui S, Rouag DA, Djukic JP, Bochet CG, Touzani R, Bailly C, Crochet A, Fromm KM (2016) Crystal structures of a copper(II) and the isotypic nickel(II) and palladium(II) complexes of the ligand (E)-1-[(2,4,6-tribromophenyl)diazenyl]naphthalen-2-ol. Acta Cryst E 72:1093

34. Zollinger H, Colour Chemistry, 2nd Edn, Weinham: VCH Publications, 1991

35. Mahapatra BB, Kumar NPA, Bhoi PK (1990) Polymetallic complexes. Part-XXX. Complexes of cobalt-, nickel-, coppery zinc-, cadmium- and mercury (II) with doubly-tridentate chelating azo-dye ligand. J Indian Chem Soc 67:800

36. Nishihara H (2005) Combination of redox-and photochemistry of azo-conjugated metal complexes. Coord Chem Rev 249:1468

37. Wang S, Shen S, Xu H, Gu D, Yin J, Tang X (2000) Spectroscopic and optical properties of an azo-metal chelate dye as optical recording medium. Mater. Sci. Eng. B76:69

38. Wang S, Shen S, Xu H, Gu D, Yin J, Tang X (1999) Synthesis and optical properties of an azo metal chelate compound for optical recording medium. Dyes Pigments 42:173

39. Mansouri L, Zouchoune B (2015) Substitution effects and electronic properties of the azo dye (1-phenylazo-2-naphthol) species: a TD-DFT electronic spectra investigation. Can J Chem 93:509

40. Humphrey SM, Wood PT (2004) Multiple areas of magnetic bistability in the topological ferrimagnet [Co₃(NC₅H₃(CO₂)₂-2, 5)₂(μ₃-OH)₂(OH₂)₂]. J Am Chem Soc 126:13236

41. Ciurtin DM, Smith MD, zur Loye HC (2003) Structural diversity in the Cu(pyrazinecarboxylate)₂/CdCl₂ system: new one-, two- and three-dimensional mixed metal coordination polymers. Dalton Trans (7):1245

42. Tong ML, Chen XM, Batten SR (2003) A new self-penetrating uniform net, (8,4) (or 8⁶), containing planar four-coordinate nodes. J Am Chem Soc 125:16170

43. Ghosh SK, Bharadwaj PK (2005) Coordination polymers of La(III) as bunched infinite nanotubes and their conversion into an open-framework structure. Inorg Chem 44:3156

44. Eubank JF, Walsh RD, Eddaoudi M (2005) Terminal co-ligand directed synthesis of a neutral, non-interpenetrated (10,3)-a metal–organic framework. Chem Commun (16):2095

45. Zhang MB, Zhang J, Zheng ST, Yang GY (2005) A 3D coordination framework based on linkages of nanosized hydroxo lanthanide clusters and copper centers by isonicotinate ligands. Angew Chem Int Ed 44:1385

46. Lu JY (2003) Crystal engineering of Cu-containing metal–organic coordination polymers under hydrothermal conditions. Coord Chem Rev 246:327

47. Farah S, Ababsa S, Benhamada N, Zouchoune B (2010) Theoretical investigation of the coordination of dibenzazepine to transition-metal complexes: a DFT study. Polyhedron 29:2722

48. Bouchakri N, Benmachiche A, Zouchoune B (2011) Bonding analysis and electronic structure of transition metal–benzoquinoline complexes: a theoretical study. Polyhedron 30:2644

49. Benmachiche A, Zendaoui SM, Bouaoud SE, Zouchoune B (2012) Electronic structure and coordination chemistry of phenanthridine ligand in first-row transition metal complexes: a DFT study. Int J Quant Chem:11985

50. Farah S, Bouchakri N, Zendaoui SM, Saillard JY, Zouchoune B (2010) Electronic structure of bis-azepine transition-metal complexes: a DFT investigation. J Mol Strut 953:143

51. Farah S, Korichi H, Zendaoui SM, Saillard JY, Zouchoune B (2009) The coordination of azepine to transition-metal complexes: a DFT analysis. Inorg Chim Acta 362:354

52. Chekkal F, Zendaoui SM, Zouchoune B, Saillard JY (2013) Structural and spin diversity of M(indenyl)$_2$transition-metal complexes: a DFT investigation. New J Chem 37:2293

53. Wang H, Xie Y, Bruce R.B, Schaefer III H.F (2008) Bis(cycloheptatrienyl) derivatives of the first-row transition metals: variable hapticity of the cycloheptatrienyl ring. Eur J Inorg Chem 23:3698

54. Zouchoune F, Zendaoui SM, Bouchakri N, Djedouani A, Zouchoune B (2010) Electronic structure and vibrational frequencies in dehydroacetic acid (DHA) transition-metal complexes: a DFT study. J Mol Struct 945:78

55. Saiad A (1096) Zouchoune B electronic (2015) structure and bonding analysis of transition metal sandwich and half-sandwich complexes of the triphenylene ligand. Can J Chem:93

56. Benhamada N, Bouchene R, Bouacida S, Zouchoune B (2015) Molecular structure, bonding analysis and redox properties of transition metal–Hapca [bis(3-aminopyrazine-2-carboxylic acid)] complexes: a theoretical study. Polyhedron 91:59

57. ADF2014.01 Version, Theoretical Chemistry, Vrije Universiteit: Amsterdam. The Netherlands, SCM

58. Baerends EJ, Ellis DE, Ros P (1973) Self-consistent molecular Hartree-Fock-Slater calculations I. The computational procedure. Chem Phys 2:41

59. te Velde G, Baerends EJ (1992) Numerical integration for poly-atomic systems. J Comput Phys 99:84

60. Fonseca Guerra C, Snijders JG, te Velde G, Baerends EJ (1998) Towards an order-N DFT method. The Chim Acc 99:391

61. Bickelhaupt FM, Baerends EJ (2000) Kohn-Sham density functional theory: predicting and understanding chemistry. Rev Comput Chem 15:1

62. te Velde G, Bickelhaupt FM, Fonseca Guerra C, van Gisbergen SJA, Baerends EJ, Snijders JG, Ziegler T (2001) Chemistry with ADF. J Comput Chem 22:931

63. Becke AD (1993) Density functional thermochemistry. III. The role of exact exchange. J Chem Phys 98:5648

64. Lee C, Yang W, Parr RG (1998) Development of the Colle-Salvetti correlation-energy formula into a functional of the electron density. Phys Rev B 37:785

65. Fan L, Ziegler T (1992) Application of density functional theory to infrared absorption intensity calculations on main group molecules. J Chem Phys 96:9005

66. Fan L, Ziegler T (1992) Application of density functional theory to infrared absorption intensity calculations on transition-metal carbonyls. J Chem Phys 96:6937

67. Runge E, Gross EKU (1984) Density-functional theory for time-dependent systems. Phys Rev Lett 52:997–1000

68. Klamt A, Schüümann G (1993) COSMO: a new approach to dielectric screening in solvents with explicit expressions for the screening energy and its gradient. J Chem Soc Perkin Trans 2:799–805

69. Flükiger P, Lüthi H.P, Portmann S, Weber J, MOLEKEL, Version 4.3.win32 Swiss Center for Scientific Computing (CSCS), Switzerland, 2000–2001. http://www.cscs.ch/molekel/

70. Ispir E (2009) The synthesis, characterization, electrochemical character, catalytic and antimicrobial activity of novel, azo-containing Schiff bases and their metal complexes. Dyes Pigments 82:13

71. Oakes J, Dixon S (2004) Physical interactions of dyes in solution – influence of dye structure on aggregation and binding to surfactants/polymers. Rev Prog Color 34:110–128

72. Alvarez J.A.L, Ruiz V.F.M, RincónJ.J, Ramírez I.M, ReyesC.F, Gutiérrez R.S, Removal of direct dyes with alginic acid. J Mex Chem Soc 59 (2015) 215–228

73. Mkpenie VN, Essien EE (2015) Solvent and methyl group effects on the electronic spectral properties of azo-2-naphtol dye. Am Chem Sci J 8(1)